Polymer-Assisted Self-Assembly of Superparamagnetic Iron Oxide Nanoparticles into Well-Defined Clusters: Controlling the Collective Magnetic Properties

ARTICLE *in* LANGMUIR · AUGUST 2014

Impact Factor: 4.46 · DOI: 10.1021/la5021934 · Source: PubMed

Langmuir

Article

pubs.acs.org/Langmuir

Polymer-Assisted Self-Assembly of Superparamagnetic Iron Oxide Nanoparticles into Well-Defined Clusters: Controlling the Collective Magnetic Properties

Christian Schmidtke,*[,†,‡] Robin Eggers,[†,‡] Robert Zierold,[§] Artur Feld,[†,‡] Hauke Kloust,[†,‡] Christopher Wolter,[†,‡] Johannes Ostermann,[†,‡] Jan-Philip Merkl,[†,‡] Theo Schotten,[∥] Kornelius Nielsch,[§] and Horst Weller*[,†,‡,∥,⊥]

[†]Institute of Physical Chemistry, University of Hamburg, Grindelallee 117, 20146 Hamburg, Germany

[‡]The Hamburg Center for Ultrafast Imaging, University of Hamburg, Luruper Chaussee 149, 22761 Hamburg, Germany

[§]Institute of Applied Physics, University of Hamburg, Jungiusstrasse 11, 20355 Hamburg, Germany

[∥]Center for Applied Nanotechnology, Grindelallee 117, 20146 Hamburg, Germany

[⊥]Department of Chemistry, Faculty of Science, King Abdulaziz University, Jeddah, Saudi Arabia

Supporting Information

ABSTRACT: The combination of superstructure-forming amphiphilic block copolymers and superparamagnetic iron oxide nanoparticles produces new nano/microcomposites with unique size-dependent properties. Herein, we demonstrate the controlled clustering of superparamagnetic iron oxide nanoparticles (SPIOs) ranging from discretely encapsulated SPIOs to giant clusters, containing hundreds or even more particles, using an amphiphilic polyisoprene-*block*-poly(ethylene glycol) diblock copolymer. Within these clusters, the SPIOs interact with each other and show new collective properties, neither obtainable with singly encapsulated nor with the bulk material. We observed cluster-size-dependent magnetic properties, influencing the blocking temperature, the magneto-viscosity of the liquid suspension, and the r_2 relaxivity for magnetic iron oxide nanoparticles. The clustering methodology can be expanded also to other nanoparticle materials [CdSe/CdS/ZnS core/shell/shell quantum dots (QDs), CdSe/CdS quantum dots/quantum rods (QDQRs), gold nanoparticles, and mixtures thereof].

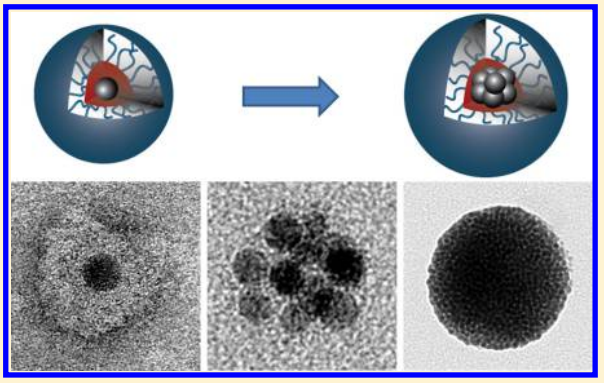

INTRODUCTION

The self-assembly of block copolymers leads to ordered superstructures (micelles, vesicles, tubules, and gels),[1,2] which can be used as vehicles for drugs or contrast agents in targeted delivery.[3] For instance, water-soluble micelles form a hydrophobic inner core, in which hydrophobic dyes or drugs can be encapsulated and well-protected.[4] The outer sphere, consisting of hydrophilic blocks, provides solubility of the micellar container and ideally minimizes interactions with the biological environment.

However, in order to exploit the outstanding size-dependent properties of inorganic nanoparticles (NPs) in material and life science,[5] these particles need to be rendered water-soluble, because high-quality NPs are usually synthesized in organic high-boiling solvents—incompatible with biological systems.

By means of block copolymers, it is possible to encapsulate the hydrophobic particles under conservation of their characteristics and render them water-soluble.[6−8] Furthermore, multiple[9] or different NPs[10] can be assembled into ordered clusters within the polymeric container.[11] This leads to new functional materials with novel collective properties (magnetic−magnetic, magnetic−plasmonic, plasmonic−plasmonic, plasmonic−fluorescent, or magnetic−fluorescent interactions) not existent in singly encapsulated NPs or in the bulk material.[12−14] Another advantage of the clustering is the signal intensity enhancement for biological imaging applications. Gaining full control over the self-assembly of NPs into well-defined monodisperse clusters is still a formidable challenge, because of multifactorial parameters influencing the self-assembly process. Clusterization depends on the nature of the polymer, the NPs-to-polymer ratio,[11,15] the solvent composition,[16] temperature, and injection speed (shearing forces[17]).

Recently, we published a report on the micellar encapsulation of NPs by using an amphiphilic poly(isoprene)-*b*-poly(ethylene glycol) diblock copolymer (PI-*b*-PEG).[18,19] This system can be further stabilized by cross-linking[20] or by introducing a

Received: June 5, 2014
Revised: August 21, 2014
Published: August 25, 2014

polystyrene shell via an emulsion polymerization process.[21] Herein, we apply our methodology for the generation of nanoparticle (NP) clusters ranging from the nano- to the microscale. We also demonstrate how clustering of iron oxide NPs affects the magnetic properties, for instance, magneto-viscosity, blocking temperature, relaxivity, and coercivity.

EXPERIMENTAL SECTION

Instrumentation. (Hydro)dynamic light scattering (DLS) measurements were performed on Malvern Zetasizer Nano ZS system equipped with a single angle 173° backscatter system using He−Ne laser illumination at 633 nm. Ultraviolet−visible (UV−vis) absorption spectra were collected on Cary 50 (Varian). Fluorescence spectra were recorded on Eclipse (Varian) and on FluoroMax-4 (Horiba) instruments. TEM-Images were recorded with a JEOL JEM-1011 microscope. SEM images were recorded with a LEO 1550 Gemini from Zeiss (Oberkochen, Germany). Flame atomic absorption spectrometry was performed on a PE 5000 spectrometer from PerkinElmer. Relaxometric measurements were performed on a Minispec mq60 (1.41 T) from Bruker Optics (Ettlingen, Germany) at 37 °C. SQUID magnetometry was conducted in a MPMS-2 system by Quantum Design enabling a magnetic field up to ±10 kOe. The cryostat temperature was controlled between 2 and 300 K with an accuracy of 1 K. A piezomembrane axial vibrator apparatus (PMAV) by IdM Ulm equipped with a magnetic coil was employed to measure the complex apparent viscosity and the shear modulus of the liquid suspensions as a function of magnetic field and shear frequency.[22] The temperature-controlled PMAV setup can handle small volumes down to 100 μL, with a maximum applied magnetic field density of 1100 Oe perpendicular to the shear flow direction. Size exclusion measurements (SEC) were performed at 35 °C on a Tosoh EcoSEC HLC-8320GPC system, using three SDV columns (Polymer Standards Service) with a porosity range from 50 to 1000 Å and a SDV precolumn with THF as solvent (1 mg/mL) and eluent. The flow rate was set to 1 mL/min and detection was executed with a Tosoh RI detector. PEG standards (PSS) were used for calibration.

Synthesis. The block copolymers [polyisoprene-*block*-diethylenetriamine (PI-DETA) and PI-*b*-PEG] (see Table 1) and the CdSe/CdS/ZnS core/shell/shell QDs were synthesized as described in ref 19.

Table 1. Analytical Data of the Copolymers

sample	M_W[a] (g/mol)	M_N[a] (g/mol)	M_W/M_N[a]	wt % PEG[b]
PI-*b*-PEG	11900	10500	1.13	67
PI-DETA	2050	1850	1.11	

[a]From SEC analysis, using a PEG calibration. [b]Calculated from NMR.

The iron oxide nanoparticles were synthesized as described by Yu et al.[23] The gold nanoparticles were synthesized according to Bastús et al.[24] The preparation of the CdSe/CdS QDQRs was performed following the protocol reported by Carbone et al.[25]

Methods. *Phase Transfer.* NPs were incubated with a 600−1000 molar excess of PI-DETA (average $M_W \sim 2$ kDa). After 3 h, NPs were precipitated with ethanol from the *n*-hexane solution and directly encapsulated by adding the PI-*b*-PEG (average $M_W \sim 11.9$ kDa) ligand. Thus, an aliquot of 20 nmol of PI-DETA-coated NPs was removed and dried under N_2 flow. The dried NPs were resuspended with a 25−400-fold excess of PI-*b*-PEG ligands in 2 mL of THF. AIBN was added in the half mass ratio as the used diblock copolymer, and three different injection methods were performed.

Phase Transfer via Syringe by Hand. This solution was injected into stirred (200 rpm) water (18 mL) via syringe and incubated for 15−30 min at room temperature. Critical step: The injection needle has to be placed into the water and the injection of air bubbles should be avoided.

Phase Transfer via Syringe Pump. This solution was injected into stirred (200 rpm) water (18 mL) via syringe pump (KDS100 from KD Scientific) and incubated for 15−30 min at room temperature. Critical step: The injection needle has to be placed into the water, and the injection of air bubbles should be avoided.

Phase Transfer via Microfluidic. The phase transfer was realized using a computer-controlled flow system (neMESYS pumps from cetoni, Gera, Germany) which is equipped with a microfluidic reactor chip as described by Thiermann et al.[26] The THF/superparamagnetic iron oxide nanoparticles (SPIOs)/polymer solution was mixed via a microfluidic chamber (microstructure = 45 μm in diameter) with water (total flow rate = 16 mL/min), whereas the flow of the THF/SPIOs/polymer phase and the water phase was always kept constant at 1:9. Afterward, the solution was incubated for 15−30 min at room temperature.

Cross-Linking. After phase transfer, the resulting solution was subsequently heated to 80 °C for 2−3 h to initiate cross-linking. The resulting NP solution was filtered through a syringe filter (CE, hydrophilic, 0.45 μm) and washed twice with 8 mL of water in centrifugal filter units (Amicon Ultra-15, 100 kDa membrane). Purification, e.g., removal of empty micelles (without NPs), was accomplished via sucrose gradient centrifugation[19] and HPLC or, in the case of iron oxide nanoparticles (FeO_X-NPs), with magnetic columns.[21]

For magnetometry and magnetorheological measurements, FeO_X-NPs−polymer clusters of three different sizes were transferred to a diethylene glycol/water mixture with a volume ratio of 7:3. The concentration of the liquid suspension was kept constant at 96 g of Fe per 1 L of carrier liquid.

Determination of the Iron Concentration. The iron concentration was determined by flame atomic absorption spectrometry. Therefore, the encapsulated SPIOs were dissolved in 32.5% nitric acid (suprapur) for 2 h at 75 °C.

Magnetization Isotherms. Magnetization isotherms were measured in an in-house-made Teflon sample holder at 2 and 300 K. Temperature-dependent measurements, namely, field-cooled (FC) and zero-field-cooled (ZFC) measurements, were conducted between 5 and 300 K with increments of 2 K. For a FC measurement a small magnetic field of 100 Oe was applied at a cryostat temperature of 300 K and the absolute magnetic moment was measured during down cooling. The ZFC procedure was performed in two steps: First, the sample was cooled from 300 to 2 K in zero magnetic field. Then, a magnetic field of 100 Oe was applied and the magnetic moment was measured during warm-up.

Magnetorheological Measurements. Magnetorheological measurements were performed by loading 100 μL of the liquid suspension into the PMAV setup. After thermal equilibration of about 10 min, the viscosity was measured at zero magnetic field and subsequently at an applied magnetic field of 1100 Oe controlled by the current flow through the magnetic coil. After an equilibration period of 10 min the measurement procedure was repeated. The absolute deviation between the two magnetoviscosity measurements was less than 1%. All measurements were carried out at 20 ± 0.2 °C.[27]

RESULTS AND DISCUSSION

Clustering of NPs was achieved by using the well-established PI-*b*-PEG diblock copolymer system with some minor modifications, namely, by varying the injection method as well as the polymer:NP ratio. The phase transfer included a three-stage process: (1) the native ligands on the NP's surface were exchanged by PI-DETA; (2) the PI-DETA-coated NPs were mixed with the PI-*b*-PEG diblock copolymer and transferred into water, under spontaneous formation of micelles, entrapping the NPs in the hydrophobic cores; and (3) the hydrophobic blocks were cross-linked by thermal treatment in the presence of a radical initiator, for instance, AIBN.[20] This led to ultrastable micelles with a fixed ligand shell around the particles. The ratio of diblock copolymers to particles determines the particle content and the final size of the micelle. A high ratio favors the formation of discretely

dx.doi.org/10.1021/la5021934 | Langmuir 2014, 30, 11190−11196

encapsulated NPs, whereas at a low ratio the relative depletion of polymer enforces particle clusterization (see Scheme 1).

Scheme 1. Schematic Representation of the PI-*b*-PEG Diblock Copolymer Encapsulation of Single or Multiple NPs

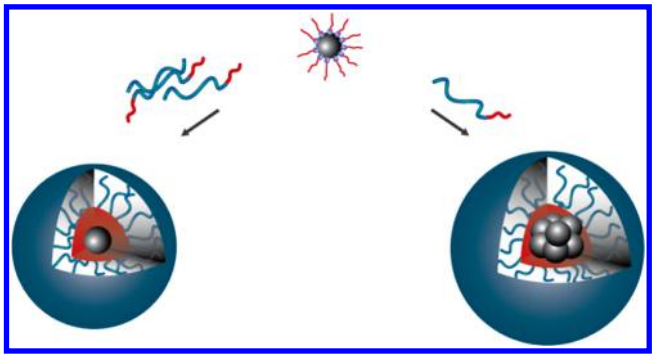

In this study, FeO_X-NPs 8 nm in diameter were coated with PI-DETA and then encapsulated with different amounts of PI-*b*-PEG diblock copolymer wiyh a polymer:NP ratio ranging from 20:1 to 400:1. Different injection methods were tested. By careful control of the conditions we were able to produce hydrodynamic diameters of FeO_X-NPs micelles from 54 to 750 nm (see Figure 1 and selected TEM/SEM overview images in the Supporting Information). In general, a 300−500-fold access of polymer per particle (with diameter between 5 and 10 nm) led predominantly to singularly encapsulated NPs, because the polymer concentration is sufficient to saturate the hydrophobic surface of the particles.[11] However, empty micelles, not enclosing any NPs, were concomitantly formed. These empty micelles and larger aggregates were removed either via sucrose gradient centrifugation and HPLC/centrifugal filter units or−if appropriate−via magnetic separation. Reversely, reduced amounts of polymer induced clustering of NP clusters, due to entropic effects of minimizing the hydrophobic surface exposed to the aqueous environment.

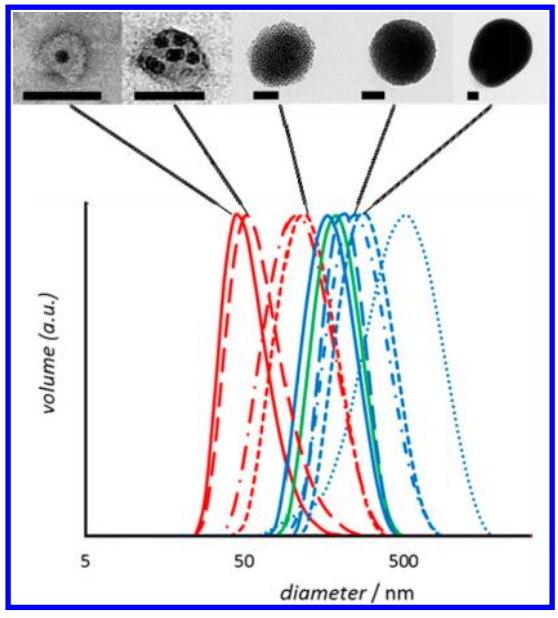

Figure 1. TEM images (scale bar = 50 nm) and hydrodynamic diameter by DLS (volume-weighted distribution) of SPIO clusters. Peak values of the curves from left to right with corresponding polymer:NP ratio and injection method (red, microfluidic mixing chamber with a flow of 16 mL/min; blue, syringe pump with a flow of 0.16 mL/min; and green, syringe via hand with a flow of 1 mL/min): 54 nm (400:1), 66 nm (200:1), 89 nm (50:1), 95 nm (30:1), 179 nm (400:1), 216 nm (50:1), 225 nm (100:1), 328 nm (50:1), 352 nm (25:1), and 747 nm (20:1).

Computer-controlled microfluidic mixing chambers (microstructure of 45 μm) provide excellent control over mixing and flow rate.[17] As a result, the reproducibility of NP micelles is greatly improved compared to the manual process. Interestingly, constant polymer:NP ratios at increased flow rates provided smaller cluster sizes, due to higher shear forces. A detailed comparison of the advantages and disadvantages of the different phase transfer methods is given in Table 2.

By using amphiphilic PI-*b*-PEG diblock polymer with a low PEG proportion of 25 wt %, large vesicular polymer−NP constructs in sizes between 0.5 and 20 μm rather than micelles were obtained, similar to previous findings.[28]

The clusterization methodology was successfully extended also to CdSe/CdS/ZnS core/shell/shell quantum dots (QDs), CdSe/CdS quantum dots/quantum mrods (QDQRs), gold NPs, and mixtures thereof, resulting in new hybrid nanomaterials (Figure 2). As expected, the collective optical properties of these micellar constructs distinctively depend on the cluster size. The absorption and emission spectra of clusters containing semiconductor QDs or QDQRs showed changes due to size-induced scattering, influencing each other mutually (possible energy transfer/cross-talk) (see Figures S7, S8, S9, and S10, Supporting Information). The clustering of plasmonic Au NPs within a micelle led as well to more scattering and to plasmon coupling (dipole moments), with a concomitant shifting of plasmon frequencies.[29,14] These findings will be reported soon. Albeit we achieved excellent control over the size of the hybrid micelles as well as the overall number of coencapsulated NPs, the composition of the heterogeneous NP payload was statistical; i.e., micelles containing different numbers of diverse NPs were obtained. The mutual physical interactions of the various heterogeneous NP collectives, e.g., QDs and Au NPs, from fluorescence quenching, energy transfer, or concurring light absorption processes,[30] imposed special challenges on the characterization of these micelle preparations.

Collective Magnetic Properties. The magnetic properties of the iron oxide clusters were studied, in particular their relaxivity, blocking temperature, and magnetoviscosity, in a suspension as a function of diameter. With increasing cluster size (i.e., aggregation number) the magnetic moment of the cluster increased. A very important application for magnetic NPs is their use as contrast agent in MRI.[31] The quality of a negative contrast agent is described by the relaxivity r_2, whereby large r_2 values are preferred. However, r_2 is determined by two counteracting phenomena resulting from aggregation number and diameter of the clusters. As described by Gillis et al. first, the relaxivity increases with increasing cluster size.[32−34] This regime is called the motional averaging regime (MAR). But with further increasing cluster size, r_2 reaches the static dephasing regime (SDR), where it stays constant and decreases in the echo limiting regime (ELR). Experimentally, the effects were examined by Pöselt et al., using a PEI-*b*-PCL-*b*-PEG triblock copolymer for the encapsulation of the FeO_X-NPs.[35] Accordingly, the PI-*b*-PEG-stabilized clusters showed a similar behavior. Clusters with hydrodynamic diameters of 54, 89, and 96 nm showed a nearly linear increase of r_2 relaxivities of 131,

dx.doi.org/10.1021/la5021934 | *Langmuir* 2014, 30, 11190−11196

Table 2. Evaluation of Different Mixing Methods

mixing method	scalability (nmol)	reproducibility	technical effort	phase of material flow
syringe by hand	20−30	moderate	low	polymer/NP/THF
syringe via pump	20−30	good	moderate	polymer/NP/THF
microfluidic	200−300	very good	high[a]	polymer/NP/THF and water

[a]Possible clogging of the microstructure under frequent use.

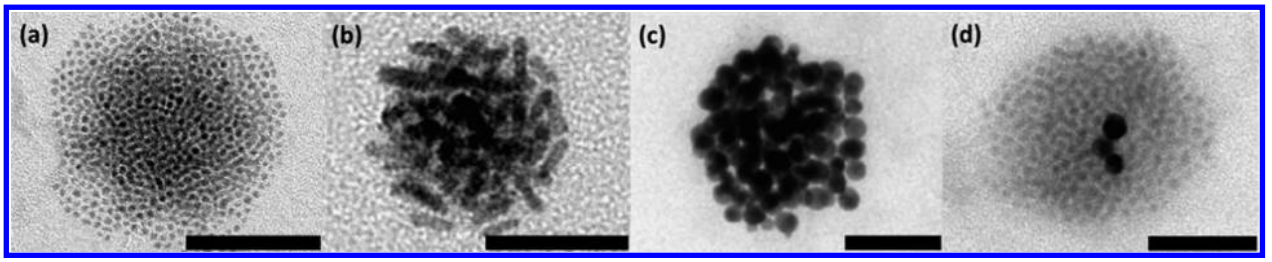

Figure 2. TEM images of clustered (a) CdSe/CdS/ZnS core/shell/shell QDs, (b) CdSe/CdS QDQRs, (c) gold NPs, and (d) QDs with gold NPs. Scale bar = 100 (a) and 50 nm (b−d).

250, and 353 mM^{-1} s^{-1}, with a sharp drop to a mere 16 mM^{-1} s^{-1} when the cluster size grew to 216 nm (DLS data).

The suspensions with cluster sizes of 54, 96, and 216 nm were subjected to SQUID magnetometry. Hysteresis curves at 5 K of all liquid suspensions (as exemplarily displayed for clusters with a hydrodynamic diameter of 216 nm in Figure 3a) displayed an open graph regarding remanence and coercive field, thus proving the permanent ferrimagnetism of the iron oxide clusters. In detail, the coercive field is increased from 32 ± 5 to 60 ± 5 Oe for increasing cluster size (Table 3). In contrast, a closed hysteresis curve is measured at 300 K without remanence and coercive field for all three studied cluster sizes. Whereas the particles are immobilized at 5 K under matrix conditions in the carrier liquid, Brownian relaxation in liquid suspension at 300 K has to be considered as a possible reason for the disappearance of coercivity and remanence. However, superparamagnetism in NPs has to be taken into account as a possible reason, too. Therefore, temperature-dependent FC and ZFC measurements [exemplarily shown in Figures 3b and S6 (Supporting Information) for the liquid suspension of 216 nm clusters] were conducted. Especially, the saturating behavior of the FC curve at low temperatures, the obvious peak in the ZFC curve (blocking temperature), and the splitting temperature of the two superimposed curves between 125 and 175 K strongly indicate superparamagnetism. Herein, the clusters (or the individual particles in the clusters) act as permanent magnets (in a blocked state) below the blocking temperature—the temperature of the peak in the ZFC curve—and become superparamagnetic (unblocked) above it. At the blocking temperature, the thermal energy exceeds the magnetic anisotropy energy of the single-domain particles, leading to a fluctuation of the magnetic moment's direction inside the individual particle.[36] Interestingly, the blocking temperature also increased with increasing cluster size (Figure 3c), as the coercive field. Since the particle size distribution in the clusters is identical in the three liquid suspensions, the determining factors are the number of particles per cluster as well as the interparticle distance. Taheri et al. have shown that similarly produced PI-DETA-coated SPIOs form well-ordered densely packing structures (body-centered cubic or face-centered cubic phases).[37] Therefore, we assume that the interparticle distance is also identical in the three samples. Differences in the interparticle distance on the TEM images can be explained as artifacts from evaporation of the stabilizing solvent and vacuum-induced flattening of the micelle on the TEM grid. Thus, the number of NPs per micelle can be regarded as the sole causation. In general, the dipolar interaction energy between nanoparticles in ensembles cannot be neglected and significantly influences the physical properties of the ensembles.[38−40] Specifically, in our case, the dipolar energy between two iron oxide nanoparticles inside one cluster is on the order of the thermal energy at the blocking temperature (further information to the calculation is given in the Supporting Information), being in good agreement with other estimations.[41] More NPs in a cluster lead to stronger dipolar interactions, which result in an increased coercive field at low temperatures, as well as to a blocking-temperature shift to higher temperatures.[42−46] Notably, as the dipolar field decreases with d^{-3} and considering the high dilution of the liquid suspension, dipolar coupling between two clusters can be neglected.

To conclude, the herein proposed synthesis route of the iron oxide−polymer clusters allows for influencing the magnetic properties of the (frozen) liquid suspension by adjusting the number of iron oxide particles per cluster. Such a precise adjustment of the low-temperature coercive field or the blocking temperature is not possible by only controlling the size of the particles: An increase of the NP diameter from 8 to 10 nm would increase the blocking temperature by more than 10 K. A controlled tuning of the collective properties of the individual clusters might be of special interest in biomedical applications like biosensing, drug delivery, and hyperthermia, to name a few of them.[47]

Magnetorheological Measurements: A Proof of Concept. Magnetic liquid suspensions based on spherical (superparamagnetic) NPs can be utilized as ferrofluids that increase their apparent viscosity (η_B) in an applied magnetic field. The viscosity increase is called magnetoviscosity (or magnetoviscous effect) and is defined as the viscosity increase normalized to the zero-field viscosity[48] (η_0): $(\eta_B - \eta_o)/(\eta_o)$.

Three liquid suspensions of PI-*b*-PEG-encapsulated SPIOs of different cluster sizes were prepared for intended biomedical use. Interestingly, when applying a magnetic field to these samples, a small but significant increase of the viscosity was detectable. Assumedly, the effect is more pronounced at iron concentrations higher than 96 mg/L Fe, chosen herein in order

dx.doi.org/10.1021/la5021934 | *Langmuir* 2014, 30, 11190−11196

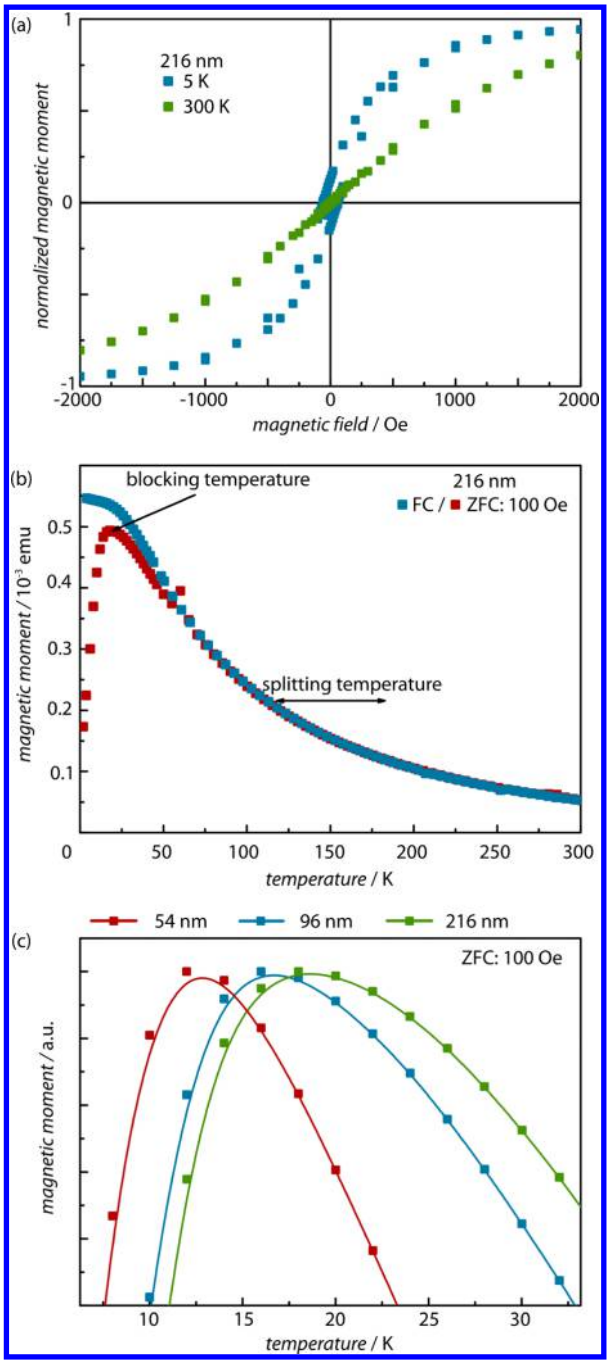

Figure 3. (a) Hysteresis curves at 5 and 300 K of SPIO clusters with a hydrodynamic diameter of 216 nm and (b) corresponding temperature-dependent FC and ZFC measurements. (c) The blocking temperature for the SPIO cluster sizes: 54 nm (red), 96 nm (blue), and 216 nm (green).

to avoid solubilization issues. This trend corresponds to magnetometry data recorded previously:[49,50] A larger cluster size results in a larger magnetoviscosity (Table 3). Remarkably, this was achieved with SPIOs of diameters as small as 8 nm. Typically, much larger SPIOs and higher Fe concentration are needed to induce these effects.

As discussed in the previous section, the individual NP diameter and the interparticle distances inside the clusters can be considered to be identical in all samples. In a future study, we will systematically vary SPIO diameters, interparticle distance, and overall iron concentration, in order to elucidate magnetoviscous effects in detail. This will open new avenues to ferrofluids with precisely controlled, tunable magnetic and magnetorheological properties.

CONCLUSION

Relaxometry, temperature-dependent magnetization, and magnetorheological measurements of defined superparamagnetic iron oxide nanoparticle clusters substantiated the relationships between cluster size (aggregation number) and the magnetic properties. In particular, it was proven that the magnetic moment per cluster is the sum of the magnetic moments of the encapsulated SPIOs and that collective effects were generated by dipolar interaction of the SPIOs within the clusters. The latter effect can be used to tune the blocking temperature, as well as the magnetoviscosity of the liquid suspension. As expected, r_2 relaxivity changed with cluster size, hence allowing the optimization of SPIO clusters as a negative contrast agent for MRT. Future investigations will elucidate the effects of nanoparticle size and interparticle distances on the magnetic properties of nanoparticular clusters in detail.

ASSOCIATED CONTENT

Supporting Information

TEM and SEM overview images of different samples of superparamagnetic iron oxide nanoparticle-clusters, a comparison of two ZFC measurements for the 216 nm cluster, details of the estimation of the dipolar energy, and absorption and emission spectra of singly and multiple encapsulated QDs/QDQRs. This material is available free of charge via the Internet at http://pubs.acs.org.

AUTHOR INFORMATION

Corresponding Authors

*C.S. e-mail: schmidtke@chemie.uni-hamburg.de.

*H.W. e-mail: weller@chemie.uni-hamburg.de.

Notes

The authors declare no competing financial interest.

ACKNOWLEDGMENTS

This work was supported by the EU within the FP 7 program (Vibrant, EU 228933), the State Excellence Initiative "Nanotechnology in Medicin", the German Research Foundation (DFG) SFB 986, the DFG Priority Program SPP 1313 (DFG WE-2059/8-2), and the DFG project NI-616/18-1. We gratefully acknowledge Prof. Carl E. Krill III, Institute of

Table 3. Magnetic Data of Different SPIO Cluster Sizes

cluster size/nm	coercive field[a]/Oe	blocking temp/K	magnetoviscosity/%
54	32	12	1.5
96	47	16	4
216	60	18	6.5

[a]At 5 K.

dx.doi.org/10.1021/la5021934 | *Langmuir* 2014, 30, 11190−11196

Micro and Nanomaterials, Ulm University, for lending the PMAV setup to the University of Hamburg. We would like to thank Dr. Neus Gómez Bastús [Institut Català de Nanotecnologia (ICN), Barcelona, Spain], Dr. Huong Tran, Dr. Jan Niehaus, Sören Becker, and Sascha Ehlert for the support and for valuable discussions. We thank Andreas Kornowski (Institute of Physical Chemistry, University of Hamburg) for the SEM images. Furthermore, we thank 2layers and specifically Frederik Schmidtke for the graphic design.

REFERENCES

(1) Förster, S.; Plantenberg, T. From Self-Organizing Polymers to Nanohybrid and Biomaterials. *Angew. Chem., Int. Ed.* **2002**, *41* (5), 688−714.

(2) Cabral, H.; Kataoka, K. Multifunctional Nanoassemblies of Block Copolymers for Future Cancer Therapy. *Sci. Technol. Adv. Mater.* **2010**, *11* (1), 014109.

(3) Blanazs, A.; Armes, S. P.; Ryan, A. J. Self-Assembled Block Copolymer Aggregates: From Micelles to Vesicles and Their Biological Applications. *Macromol. Rapid Commun.* **2009**, *30* (4-5), 267−277.

(4) Oerlemans, C.; Bult, W.; Bos, M.; Storm, G.; Nijsen, J. F.; Hennink, W. Polymeric Micelles in Anticancer Therapy: Targeting, Imaging and Triggered Release. *Pharm. Res.* **2010**, *27* (12), 2569−2589.

(5) Burda, C.; Chen, X.; Narayanan, R.; El-Sayed, M. A. Chemistry and Properties of Nanocrystals of Different Shapes. *Chem. Rev.* **2005**, *105* (4), 1025−1102.

(6) Dubertret, B.; Skourides, P.; Norris, D. J.; Noireaux, V.; Brivanlou, A. H.; Libchaber, A. In Vivo Imaging of Quantum Dots Encapsulated in Phospholipid Micelles. *Science* **2002**, *298* (5599), 1759−1762.

(7) Pellegrino, T.; Manna, L.; Kudera, S.; Liedl, T.; Koktysh, D.; Rogach, A. L.; Keller, S.; Rädler, J.; Natile, G.; Parak, W. J. Hydrophobic Nanocrystals Coated with an Amphiphilic Polymer Shell: A General Route to Water Soluble Nanocrystals. *Nano Lett.* **2004**, *4* (4), 703−707.

(8) Kang, Y.; Taton, T. A. Core/Shell Gold Nanoparticles by Self-Assembly and Crosslinking of Micellar, Block-Copolymer Shells. *Angew. Chem., Int. Ed.* **2005**, *44* (3), 409−412.

(9) Kim, B.-S.; Qiu, J.-M.; Wang, J.-P.; Taton, T. A. Magnetomicelles: Composite Nanostructures from Magnetic Nanoparticles and Cross-Linked Amphiphilic Block Copolymers. *Nano Lett.* **2005**, *5* (10), 1987−1991.

(10) Kim, B.-S.; Taton, T. A. Multicomponent Nanoparticles Via Self-Assembly with Cross-Linked Block Copolymer Surfactants. *Langmuir* **2006**, *23* (4), 2198−2202.

(11) Rhyner, M. N.; Smith, A.; Nie, S. Micellar Structures, Methods of Making Micellar Structures, Methods of Imaging, and Methods of Delivering Agents. WO patent: WO2008137733 A3, 2008.

(12) He, J.; Liu, Y.; Babu, T.; Wei, Z.; Nie, Z. Self-Assembly of Inorganic Nanoparticle Vesicles and Tubules Driven by Tethered Linear Block Copolymers. *J. Am. Chem. Soc.* **2012**, *134* (28), 11342−11345.

(13) Li, W.; Liu, S.; Deng, R.; Wang, J.; Nie, Z.; Zhu, J. A Simple Route to Improve Inorganic Nanoparticles Loading Efficiency in Block Copolymer Micelles. *Macromolecules* **2013**, *46* (6), 2282−2291.

(14) Sánchez-Iglesias, A.; Grzelczak, M.; Altantzis, T.; Goris, B.; Pérez-Juste, J.; Bals, S.; Van Tendeloo, G.; Donaldson, S. H.; Chmelka, B. F.; Israelachvili, J. N.; Liz-Marzán, L. M. Hydrophobic Interactions Modulate Self-Assembly of Nanoparticles. *ACS Nano* **2012**, *6* (12), 11059−11065.

(15) Sanchez-Gaytan, B. L.; Cui, W.; Kim, Y.; Mendez-Polanco, M. A.; Duncan, T. V.; Fryd, M.; Wayland, B. B.; Park, S.-J. Interfacial Assembly of Nanoparticles in Discrete Block-Copolymer Aggregates. *Angew. Chem.* **2007**, *119* (48), 9395−9398.

(16) Hickey, R. J.; Haynes, A. S.; Kikkawa, J. M.; Park, S.-J. Controlling the Self-Assembly Structure of Magnetic Nanoparticles and Amphiphilic Block-Copolymers: From Micelles to Vesicles. *J. Am. Chem. Soc.* **2011**, *133* (5), 1517−1525.

(17) Wang, C.-W.; Oskooei, A.; Sinton, D.; Moffitt, M. G. Controlled Self-Assembly of Quantum Dot−Block Copolymer Colloids in Multiphase Microfluidic Reactors. *Langmuir* **2009**, *26* (2), 716−723.

(18) Pöselt, E.; Schmidtke, C.; Fischer, S.; Peldschus, K.; Salamon, J.; Kloust, H.; Tran, H.; Pietsch, A.; Heine, M.; Adam, G.; Schumacher, U.; Wagener, C.; Förster, S.; Weller, H. Tailor-Made Quantum Dot and Iron Oxide Based Contrast Agents for in Vitro and in Vivo Tumor Imaging. *ACS Nano* **2012**, *6* (4), 3346−3355.

(19) Schmidtke, C.; Pöselt, E.; Ostermann, J.; Pietsch, A.; Kloust, H.; Tran, H.; Schotten, T.; Bastús, N. G.; Eggers, R.; Weller, H. Amphiphilic, Cross-Linkable Diblock Copolymers for Multifunctionalized Nanoparticles as Biological Probes. *Nanoscale* **2013**, *5* (16), 7433−7444.

(20) Schmidtke, C.; Lange, H.; Tran, H.; Ostermann, J.; Kloust, H.; Bastús, N. G.; Merkl, J.-P.; Thomsen, C.; Weller, H. Radical Initiated Reactions on Biocompatible CdSe-Based Quantum Dots: Ligand Cross-Linking, Crystal Annealing, and Fluorescence Enhancement. *J. Phys. Chem. C* **2013**, *117* (16), 8570−8578.

(21) Kloust, H.; Schmidtke, C.; Feld, A.; Schotten, T.; Eggers, R.; Fittschen, U. E. A.; Schulz, F.; Pöselt, E.; Ostermann, J.; Bastús, N. G.; Weller, H. In Situ Functionalization and PEO Coating of Iron Oxide Nanocrystals Using Seeded Emulsion Polymerization. *Langmuir* **2013**, *29* (15), 4915−4921.

(22) Kirschenmann, L. Aufbau Zweier Piezoelektrischer Sonden (PRV/PAV) Zur Messung der Viskoelastischen Eigenschaften Weicher Substanzen im Frequenzbereich 0,5 Hz−2 kHz bzw. 0,5 Hz−7 kHz. Ph.D. thesis, Ulm University, Ulm, Germany, 2003.

(23) Yu, W. W.; Falkner, J. C.; Yavuz, C. T.; Colvin, V. L. Synthesis of Monodisperse Iron Oxide Nanocrystals by Thermal Decomposition of Iron Carboxylate Salts. *Chem. Commun.* **2004**, *20*, 2306−2307.

(24) Bastús, N. G.; Comenge, J.; Puntes, V. Kinetically Controlled Seeded Growth Synthesis of Citrate-Stabilized Gold Nanoparticles of up to 200 nm: Size Focusing Versus Ostwald Ripening. *Langmuir* **2011**, *27* (17), 11098−11105.

(25) Carbone, L.; Nobile, C.; De Giorgi, M.; Sala, F. D.; Morello, G.; Pompa, P.; Hytch, M.; Snoeck, E.; Fiore, A.; Franchini, I. R.; Nadasan, M.; Silvestre, A. F.; Chiodo, L.; Kudera, S.; Cingolani, R.; Krahne, R.; Manna, L. Synthesis and Micrometer-Scale Assembly of Colloidal CdSe/CdS Nanorods Prepared by a Seeded Growth Approach. *Nano Lett.* **2007**, *7* (10), 2942−2950.

(26) Thiermann, R.; Mueller, W.; Montesinos-Castellanos, A.; Metzke, D.; Löb, P.; Hessel, V.; Maskos, M. Size Controlled Polymersomes by Continuous Self-Assembly in Micromixers. *Polymer* **2012**, *53* (11), 2205−2210.

(27) Wu, Z.; Zierold, R.; Mueller, A.; Ruff, S. E.; Ma, C.; Khan, A. A.; Geiger, F.; Sommer, B. A.; Knez, M.; Nielsch, K.; Bittner, A. M.; Wege, C.; Krill, C. E. Preparation and Magnetoviscosity of Nanotube Ferrofluids by Viral Scaffolding and ALD on Porous Templates. *Phys. Status Solidi B* **2010**, *247* (10), 2412−2423.

(28) Krack, M.; Hohenberg, H.; Kornowski, A.; Lindner, P.; Weller, H.; Förster, S. Nanoparticle-Loaded Magnetophoretic Vesicles. *J. Am. Chem. Soc.* **2008**, *130* (23), 7315−7320.

(29) Murphy, C. J.; Gole, A. M.; Stone, J. W.; Sisco, P. N.; Alkilany, A. M.; Goldsmith, E. C.; Baxter, S. C. Gold Nanoparticles in Biology: Beyond Toxicity to Cellular Imaging. *Acc. Chem. Res.* **2008**, *41* (12), 1721−1730.

(30) Schmidtke, C.; Kloust, H.; Bastús, N. G.; Merkl, J.-P.; Tran, H.; Flessau, S.; Feld, A.; Schotten, T.; Weller, H. A General Route towards Well-Defined Magneto- or Fluorescent-Plasmonic Nanohybrids. *Nanoscale* **2013**, *5* (23), 11783−94.

(31) Na, H. B.; Song, I. C.; Hyeon, T. Inorganic Nanoparticles for MRI Contrast Agents. *Adv. Mater.* **2009**, *21* (21), 2133−2148.

(32) Gillis, P.; Moiny, F.; Brooks, R. A. On T2-Shortening by Strongly Magnetized Spheres: A Partial Refocusing Model. *Magn Reson Med.* **2002**, *47* (2), 257−263.

(33) Gossuin, Y.; Gillis, P.; Hocq, A.; Vuong, Q. L.; Roch, A. Magnetic Resonance Relaxation Properties of Superparamagnetic

Particles. *Wiley Interdiscip. Rev.: Nanomed. Nanobiotechnol.* **2009**, *1* (3), 299−310.
(34) Vuong, Q. L.; Gillis, P.; Gossuin, Y. Monte Carlo Simulation and Theory of Proton NMR Transverse Relaxation Induced by Aggregation of Magnetic Particles Used as MRI Contrast Agents. *J. Magn. Reson.* **2011**, *212* (1), 139−148.
(35) Pöselt, E.; Kloust, H.; Tromsdorf, U.; Janschel, M.; Hahn, C.; Maßlo, C.; Weller, H. Relaxivity Optimization of a PEGylated Iron-Oxide-Based Negative Magnetic Resonance Contrast Agent for T2-Weighted Spin−Echo Imaging. *ACS Nano* **2012**, *6* (2), 1619−1624.
(36) Knobel, M.; Nunes, W. C.; Socolovsky, L. M.; De Biasi, E.; Vargas, J. M.; Denardin, J. C. Superparamagnetism and Other Magnetic Features in Granular Materials: A Review on Ideal and Real Systems. *J. Nanosci. Nanotechnol.* **2008**, *8* (6), 2836−2857.
(37) Taheri, S. M.; Fischer, S.; Trebbin, M.; With, S.; Schröder, J. H.; Perlich, J.; Roth, S. V.; Forster, S. Lyotropic Phase Behavior of Polymer-Coated Iron Oxide Nanoparticles. *Soft Matter* **2012**, *8* (48), 12124−12131.
(38) García-Otero, J.; Porto, M.; Rivas, J.; Bunde, A. Influence of Dipolar Interaction on Magnetic Properties of Ultrafine Ferromagnetic Particles. *Phys. Rev. Lett.* **2000**, *84* (1), 167−170.
(39) Poddar, P.; Telem-Shafir, T.; Fried, T.; Markovich, G. Dipolar Interactions in Two- and Three-Dimensional Magnetic Nanoparticle Arrays. *Phys. Rev. B* **2002**, *66* (6), 060403−1-060403-4.
(40) Hiroi, K.; Komatsu, K.; Sato, T. Superspin Glass Originating from Dipolar Interaction with Controlled Interparticle Distance among γ-Fe_2O_3 Nanoparticles with Silica Shells. *Phys. Rev. B* **2011**, *83* (22), 224423-1−224423-9.
(41) Varón, M.; Beleggia, M.; Kasama, T.; Harrison, R. J.; Dunin-Borkowski, R. E.; Puntes, V. F.; Frandsen, C. Dipolar Magnetism in Ordered and Disordered Low-Dimensional Nanoparticle Assemblies. *Sci. Rep.* **2013**, *3*, 1−5.
(42) Mørup, S.; Hansen, M. F.; Frandsen, C. Magnetic Interactions between Nanoparticles. *Beilstein J. Nanotechnol.* **2010**, *1*, 182−190.
(43) Bae, C. J.; Angappane, S.; Park, J.-G.; Lee, Y.; Lee, J.; An, K.; Hyeon, T. Experimental Studies of Strong Dipolar Interparticle Interaction in Monodisperse Fe_3O_4 Nanoparticles. *Appl. Phys. Lett.* **2007**, *91* (10), 102502-1−102502-3.
(44) Dormann, J. L.; D'Orazio, F.; Lucari, F.; Tronc, E.; Prené, P.; Jolivet, J. P.; Fiorani, D.; Cherkaoui, R.; Noguès, M. Thermal Variation of the Relaxation Time of the Magnetic Moment of γ-Fe_2O_3 Nanoparticles with Interparticle Interactions of Various Strengths. *Phys. Rev. B* **1996**, *53* (21), 14291−14297.
(45) Nunes, W. C.; Cebollada, F.; Knobel, M.; Zanchet, D. Effects of Dipolar Interactions on the Magnetic Properties of γ-Fe_2O_3 Nanoparticles in the Blocked State. *J. Appl. Phys.* **2006**, *99* (8), 08N705-1−08N705-3.
(46) Peddis, D.; Orrù, F.; Ardu, A.; Cannas, C.; Musinu, A.; Piccaluga, G. Interparticle Interactions and Magnetic Anisotropy in Cobalt Ferrite Nanoparticles: Influence of Molecular Coating. *Chem. Mater.* **2012**, *24* (6), 1062−1071.
(47) Kolhatkar, A. G.; Jamison, A. C.; Litvinov, D.; Willson, R. C.; Lee, T. R. Tuning the Magnetic Properties of Nanoparticles. *Int. J. Mol. Sci.* **2013**, *14*, 15977−16009.
(48) Odenbach, S. Recent Progress in Magnetic Fluid Research. *J. Phys.: Condens. Matter* **2004**, *16* (32), R1135.
(49) Odenbach, S.; Raj, K. The Influence of Large Particles and Agglomerates on the Magnetoviscous Effect in Ferrofluids. *Magnetohydrodynamics* **2000**, *36* (4), 312−319.
(50) Thurm, S.; Odenbach, S. Particle Size Distribution as Key Parameter for the Flow Behavior of Ferrofluids. *Phys. Fluids* **2003**, *15* (6), 1658−1664.